Mattila, Nina; Karttunen, Antti J.

Electronic Properties and Lattice Dynamics of Li_xCoO_2 and Na_xCoO_2 (x = 0, 0.5, 1) Studied by Hybrid Density Functional Theory

Published in:
Physica Status Solidi (B) Basic Research

DOI:
10.1002/pssb.202100665

Published: 01/04/2022

Document Version
Publisher's PDF, also known as Version of record

Please cite the original version:
Mattila, N., & Karttunen, A. J. (2022). Electronic Properties and Lattice Dynamics of Li_xCoO_2 and Na_xCoO_2 (x = 0, 0.5, 1) Studied by Hybrid Density Functional Theory. *Physica Status Solidi (B) Basic Research*, *259*(4), Article 2100665. https://doi.org/10.1002/pssb.202100665

Check for updates

RESEARCH ARTICLE

60 years of pss

physica status solidi b

www.pss-b.com

Electronic Properties and Lattice Dynamics of Li_xCoO_2 and Na_xCoO_2 ($x = 0, 0.5, 1$) Studied by Hybrid Density Functional Theory

*Nina Mattila and Antti J. Karttunen**

A systematic hybrid density functional theory study on the electronic and vibrational properties of M_xCoO_2 compounds with M = Li, Na and $x = 0, 0.5, 1$ is reported. The used DFT-PBE0 method describes the structural parameters of the studied compounds well in comparison to experimental data. All studied magnetic species are treated as ferromagnets and the Co(IV) atoms possess a magnetic moment of 1.2 μ_B. At 0 K, CoO_2 favors a monoclinic structure very close to trigonal symmetry and behaves as a Mott insulator. The electronic bandgap increases as x increases from 0 to 1. The simulated infrared and Raman spectra together with full phonon dispersion relations show that the intercalation of Li and Na ions affects the lattice dynamics of CoO_2 in a different way.

1. Introduction

Layered alkali metal oxides Li_xCoO_2 and Na_xCoO_2 are representatives of the vast group of compounds derived from the layered parent compound CoO_2 (see **Figure 1**). The Co–O layers in these compounds are formed by edge-sharing CoO_6 octahedra. It is well known that the electronic and magnetic properties of Li_xCoO_2 and Na_xCoO_2 are very dependent on the alkali metal composition (x) and they have attracted a lot of scientific and technological interest, for example, as Li-ion battery materials and thermoelectric energy conversion materials.[1–7]

Even though Li_xCoO_2 and Na_xCoO_2 have been extensively studied both experimentally and computationally, there have been some differences in the reported electronic and magnetic properties. In the case of CoO_2, the $x = 0$ end member, each Co(IV) atom would possess one unpaired electron in the low-spin d^5 configuration. CoO_2 without alkali metals was first reported by Amatucci et al. in 1996. They obtained the compound via chemical deintercalation of $LiCoO_2$ and reported it to be a nonmagnetic metal.[8,9] In 2007, Motohashi et al. synthesized CoO_2 by electrochemical deintercalation of $LiCoO_2$ and reported it to be Pauli paramagnetic metal with itinerant electrons.[10] Vaulx et al. studied CoO_2 with ^{59}Co NMR and described it as a metal, while magnetic susceptibility measurements revealed antiferromagnetic spin fluctuations and suggested the vicinity of a Mott insulator transition at low temperatures of about 7 K.[11] Kawasaki et al. also studied CoO_2 using ^{59}Co nuclear magnetic resonance (NMR) together with nuclear quadrupole resonance (NQR).[12] They reported CoO_2 to be a non-correlated metal satisfying Korringa law for a Fermi liquid and reproduced the findings of Vaulx et al. for a $Li_{0.12}CoO_2$ sample.

Theoretical studies on CoO_2 have also produced rather varying results. Zhang et al. studied the electronic and structural properties of a single CoO_2 layer with density functional theory (DFT) within the local spin density approximation and U correction (DFT-LSDA+U). As expected, they observed a strong dependency on the U correction. LSDA+U with $U = 5.5$ eV resulted in CoO_2 being a charge transfer insulator with Co(IV) magnetic moment μ of about 1 μ_B. With plain LSDA, CoO_2 was a metal with high density of states (DOS) at the Fermi level and μ of 0.58 μ_B.[13] Lee and Pickett studied the strength of correlation effects in $Na_xCoO_2 \rightarrow 0$ using LSDA+U. Comparing their results with the experimental observations of Amatucci et al.,[8] they concluded that U has to be smaller than 2.3 eV to obtain a nonmagnetic metal, while above 2.3 eV a Mott insulating state is obtained.[9]

Half-filled $Na_{0.5}CoO_2$ possesses remarkable electronic properties and has been studied intensively. Terasaki et al. studied the transport properties of a single crystal.[4] Similar to previous reports,[14] they described the compound as metallic, with in-plane thermopower of 100 $\mu V K^{-1}$ at room temperature and low resistivity of 200 $\mu\Omega$ cm, making it a promising thermoelectric material. They also observed high electrical anisotropy and described a metal–semiconductor transition in the cross-plane at 200 K.

Ray et al. proposed a possible magnetic structure for $Na_{0.5}CoO_2$ based on ^{23}Na and ^{59}Co NMR studies, suggesting that the magnetic Co(IV) atoms alternate with diamagnetic Co(III) atoms.[15] In 2004, Foo et al. reported the phase diagram of Na_xCoO_2 for $0.3 \leq x \leq 0.75$.[5] According to their results, Na_xCoO_2 is generally a metal for whole doping range except for the half-filled $Na_{0.5}CoO_2$ where charge-ordered insulating state separates the low-doped paramagnetic phase and the highly doped Curie–Weiss metallic

N. Mattila, A. J. Karttunen
Department of Chemistry and Materials Science
Aalto University
P.O. Box 16100, FI-00076 Aalto, Finland
E-mail: antti.j.karttunen@iki.fi

The ORCID identification number(s) for the author(s) of this article can be found under https://doi.org/10.1002/pssb.202100665.

DOI: 10.1002/pssb.202100665

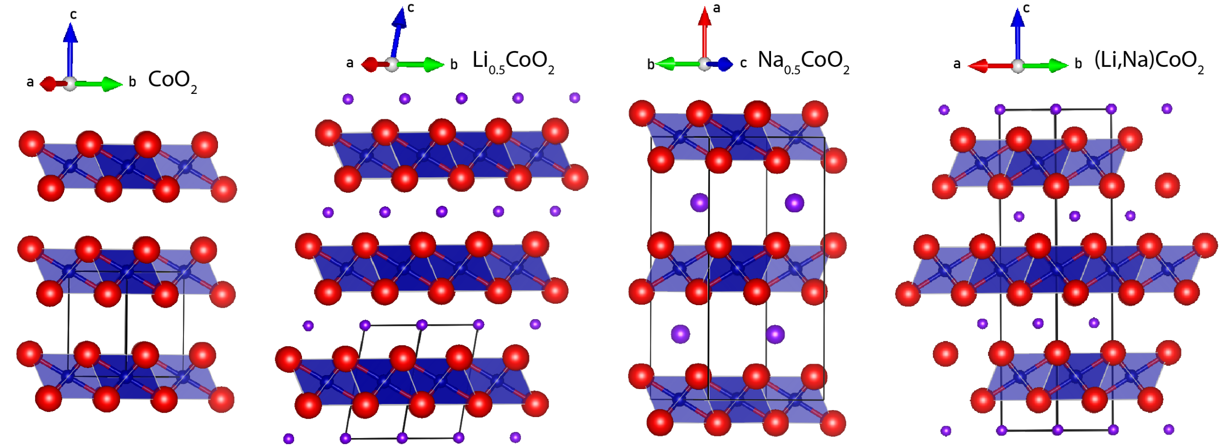

Figure 1. Crystal structures of the studied M_xCoO_2 structures. Blue: Co; red: O; purple: Li/Na.

phase. At the doping level of $x = 0.75$, weak magnetization explained by spin density wave occurs.[16]

Huang et al. conducted electronic, magnetic, and specific heat measurements on $Na_{0.5}CoO_2$ and observed phase transitions at temperatures of 87, 53, and 20 K.[17] Similar phenomena were reported by Viciu et al. who studied Na_xCoO_2 compounds with $0.32 \leq x \leq 0.92$.[18] The orthorhombic crystal structure determined for $Na_{0.5}CoO_2$ leads in two symmetry-independent Co sites and an insulating charge-ordered state. Williams et al. have noted that the diffraction data reported for $Na_{0.5}CoO_2$ were insufficient for full understanding of the CoO_2 lattice.[19] They studied $Na_{0.5}CoO_2$ within high-resolution powder neutron diffraction at temperatures 10–300 K, concluding that the electron density of the two Co sites is only slightly different and a conventional charge-ordered state might not be a proper model.

From a computational point of view, Singh applied DFT-LDA to study electronic and magnetic properties of $Na_{0.5}CoO_2$.[20] The paramagnetic metallic hexagonal structure proposed by Jansen and Hoppe,[21] with arbitrarily placed Na atoms, was used as a starting point. DFT-LSDA yielded a half-metallic ferromagnetic configuration with magnetic moment of 0.5 μ_B per Co.

Turning to Li_xCoO_2, Hertz et al. investigated the magnetic properties and structure of Li_xCoO_2 for $0.5 < x < 1$.[22] From the magnetic susceptibility measurements, they observed a small anomaly for some samples at 175 K, apart from which all Li_xCoO_2 samples exhibited Curie–Weiss behavior. Remeasurement of same samples after 4 months revealed significant suppression of the anomaly and therefore it was proposed that origin of the anomaly can be a small impurity phase slowly decomposing in air, or subtle structure defect that diminishes in time, e.g., through homogeneous Li^+ distribution. From small negative values of Curie–Weiss temperature Θ_w, they concluded that Li_xCoO_2 at $0.5 < x < 1$ exhibits a small antiferromagnetic behavior increasing with Li deintercalation and low spin–high spin Co(IV) transition at $x > 0.5$. The structure of Li_xCoO_2 was thoroughly analyzed by neutron diffraction methods and revealed significant structural differences of CoO_2 layers compared with Li_xCoO_2, implying higher distortion of CoO_6 octahedra in Li_xCoO_2.

The electronic phase diagram of Li_xCoO_2 reported by Motohashi et al. has seven stable phases and appears more complicated in comparison to Li_xCoO_2.[23] Starting from CoO_2, Li_xCoO_2 is Pauli paramagnetic metal up to $x = 0.35$. Lithium intercalation increases the energy of the conduction band and the number of nonmagnetic Co(III) ions. Li_xCoO_2 with $0.40 \leq x \leq 0.70$ is generally discussed as a Curie–Weiss metal which turns to a band semiconductor with further intercalation. The end member $LiCoO_2$ is a nonmagnetic band insulator. We have discussed the literature related to the fully intercalated, nonmagnetic $LiCoO_2$ and $NaCoO_2$ in a recent article and will not repeat them here.[24]

Here, we investigate the electronic properties and lattice dynamics of layered alkali metal oxides Li_xCoO_2 and Na_xCoO_2 using hybrid density functional methods. We study the effect of the doping level x ($x = 0, 0.5, 1$) and the alkali metal type (Li vs Na). Using the same hybrid density functional method for all studied compounds enables the systematic comparison of the trends in the electronic, magnetic, and vibrational properties.

2. Results

2.1. Geometry and Magnetic Ordering

The optimized lattice parameters of the Co atom are reported in **Table 1** (DFT-PBE0 method, see Computational Details). The optimized lattice parameters compare well with the experimental values, except for the c parameter of CoO_2, which is overestimated

Table 1. Optimized lattice parameters a, b, and c of the studied systems in Å. The numbers in the parentheses show the deviation from the experimental values in percentages (%).[5,23,50,51] The lattice parameters of CoO_2 refer to the primitive cell.

	CoO_2	$Li_{0.5}CoO_2$	$Na_{0.5}CoO_2$	$LiCoO_2$	$NaCoO_2$
	($C12/m1$)	($P12/m1$)	($Pmmn$)	($R\bar{3}m$)	($R\bar{3}m$)
a	2.80 (−0.6)	4.83 (−0.7)	4.84 (−0.8)	2.80 (−0.5)	2.87 (−0.6)
b	2.80 (−0.6)	2.79 (−0.6)	5.61 (−0.4)	2.80 (−0.5)	2.87 (−0.6)
c	4.42 (+4.2)	5.13 (+1.4)	11.05 (−0.1)	13.98 (−0.5)	15.62 (+0.1)

by 4.2% despite the D3 dispersion correction. We also benchmarked the D3 dispersion correction with Becke–Johnson damping, but this led in even larger overestimation by 5.1%. The lattice parameters and coordinates of the optimized structures are given as Supporting Information.[25] The magnetic moment of the Co(IV) ion is practically the same 1.2 μ_B for all materials.

While the ideal space group of the end member CoO_2 is $P\bar{3}m1$, this structure is not a true local minimum at the DFT-PBE0-D3/TZVP level of theory, as a Γ-point frequency calculation revealed a twofold degenerate imaginary vibrational frequency of $-414\,cm^{-1}$ (at 0 K). The c lattice parameter of the trigonal geometry is 4.02 Å, which is underestimated by over 5% compared to the experiment. Lowering the symmetry to monoclinic subgroup $C12/m1$ leads in a structure that is close to the original trigonal structure and in reasonable agreement with the experimental lattice constants (lattice parameter c is overestimated). The monoclinic structure is $-0.2\,kJ\,mol^{-1}$ lower in energy and does not show any imaginary frequencies. We studied both ferromagnetic (FM) and antiferromagnetic (AFM) magnetic ordering for CoO_2. To achieve an AFM ordering, we had to create a supercell, ending up in $P\bar{1}$ space group. The AFM ordering is slightly lower in energy in comparison to the FM ordering ($2\,kJ\,mol^{-1}$), but we carried out the majority of our calculations using the higher symmetry FM ordering to enable comparisons with the intercalated systems and the experiments. The structural and magnetic details of the antiferromagnetic configuration are reported in the Supporting Information.

Na-intercalated $Na_{0.5}CoO_2$ crystallizes in orthorhombic space group $Pmmn$ and has both nonmagnetic Co(III) and magnetic Co(IV) ions. We tested both FM and AFM ordering for $Na_{0.5}CoO_2$ (for AFM, the symmetry had to be reduced to $P12_1/m1$). The energy difference between FM and AFM is very small; FM is $0.2\,kJ\,mol^{-1}$ lower in energy. We used the higher symmetry FM configuration in our calculations. The structural and magnetic details of the antiferromagnetic configuration are reported in the Supporting Information. FM ordering was also used for the magnetic Co(IV) ions in the lithium-intercalated $Li_{0.5}CoO_2$ crystallizing in lower symmetry monoclinic space group $P12/m1$. The nonmagnetic end members $LiCoO_2$ and $NaCoO_2$ both crystallize in a trigonal crystal structure ($R\bar{3}m$). The alkali metal ions occupy octahedral sites between the oxygen atoms of the adjacent layers.

2.2. Band Structures

The electronic band structures are presented in **Figure 2** and **3** for magnetic and nonmagnetic compounds, respectively. At 0 K, the CoO_2 end member is an insulator with a bandgap of 2.9 and 2.8 eV for α and β spin channels, respectively, suggesting Mott insulator-type situation.[11] Topmost valence bands are dominated by oxygen and the lowest energy conduction band of the β spin channel is dominated by Co, as expected. If nonhybrid DFT-PBE method is used for CoO_2, the optimized lattice parameters agree well with experiments (difference of +0.2% and +1.9% for a and c, respectively), but the system is metallic at 0 K. The optimized lattice parameter c of CoO_2 appears to be rather sensitive with respect to the electronic ground state.

Alkali metal intercalation into CoO_2 increases the bandgap. For the $x = 0.5$ systems, the increase is still rather small: the α and β spin channel band gaps are 3.1 and 2.8 eV for $Li_{0.5}CoO_2$ and 3.0 and 2.8 eV for $Na_{0.5}CoO_2$. The contribution from the Li and Na ions to the DOS is negligible both for the topmost valence bands and the lowest energy conduction bands. The fully intercalated end members $LiCoO_2$ and $NaCoO_2$ show the largest bandgaps of 4.9 and 4.8 eV, respectively.

2.3. IR and Raman Spectroscopy

We calculated the harmonic vibrational frequencies at the Γ-point for all studied systems, together with IR and Raman intensities. The number of optical modes for different systems is as follows: CoO_2: 6; $Li_{0.5}CoO_2$: 18; $Na_{0.5}CoO_2$: 81; $(Li,Na)CoO_2$: 6. The calculated IR and Raman spectra are plotted in **Figure 4** and full details are given in tabulated form in the Supporting Information.[25]

Direct comparisons of the spectra of different materials are complicated by the differences in their symmetry properties. However, it is possible to observe the general trends on how the spectra of CoO_2 change as result of alkali metal intercalation.

In the case of Li_xCoO_2, the low-energy IR-active peaks 100–300 cm^{-1} arise from the alkali atoms, while the modes at 500–700 cm^{-1} represent modes of the CoO_6 octahedra (Co—O bond stretching, O—Co—O bending and twisting, etc.). The modes at 300–400 cm^{-1} involve both Li atoms and CoO_2 layers. As expected, based on their atomic masses, the energy of the modes involving Li is higher than that for Na. The modes of Na_xCoO_2 can be described as follows: Na atom vibrates in the range 100–200, 200–300 cm^{-1} range involves both Na atoms CoO_2 layers, and the modes at 500–700 cm^{-1} range arise from the CoO_2 layers. The intensity difference of Li- and Na-based modes can be observed for $LiCoO_2$ and $NaCoO_2$ at the range 100–500 cm^{-1}.

The alkali metal-based modes are less visible in Raman spectra compared to the IR spectra. For all compounds, mainly modes in the range 400–700 cm^{-1}, arising from CoO_2 layers, are clearly visible. Only in $Na_{0.5}CoO_2$, low-intensity Na-based modes can be observed at 100–300 cm^{-1}.

Yang et al. have conducted Raman measurements for $Na_{0.5}CoO_2$ single crystal at various temperatures. They observed phase transition upon cooling from high-temperature hexagonal structure to the orthorhombic low-temperature structure, starting at about 200 K.[26] In the spectrum obtained at 80 K, they observed only three Raman peaks at 439, 476, and 573 cm^{-1}. Later, Zhang et al. reported five Raman peaks at 10 K: 414, 437, 475, 497 (low intensity), and 570 cm^{-1}.[27]

The in-plane infrared reflectance of a $Na_{0.5}CoO_2$ single crystal has been studied by Wang et al. at various temperatures.[28] They observed a charge-ordered state appearing with lowering temperature to 100 K, followed by a charge density wave that is responsible for metal–insulator transition at 50 K. They reported IR-active peaks at 10 K with frequencies of 102, 282, 435, 530, and 535 cm^{-1}. Lupi et al. measured in-plane infrared conductivity of Na_xCoO_2 $0.5 \leq x \leq 1$ as a function of x and temperature.[29] The spectrum obtained at 12 K is similar with the spectrum presented here: peaks at about 180–400 cm^{-1} vanish with increasing x, while the peak at 590 cm^{-1} is visible for all cases, but decreases in intensity with increasing x. The slightly metallic behavior observed at low temperatures for nominally insulating $NaCoO_2$ was ascribed to nonstoichiometry. A detailed

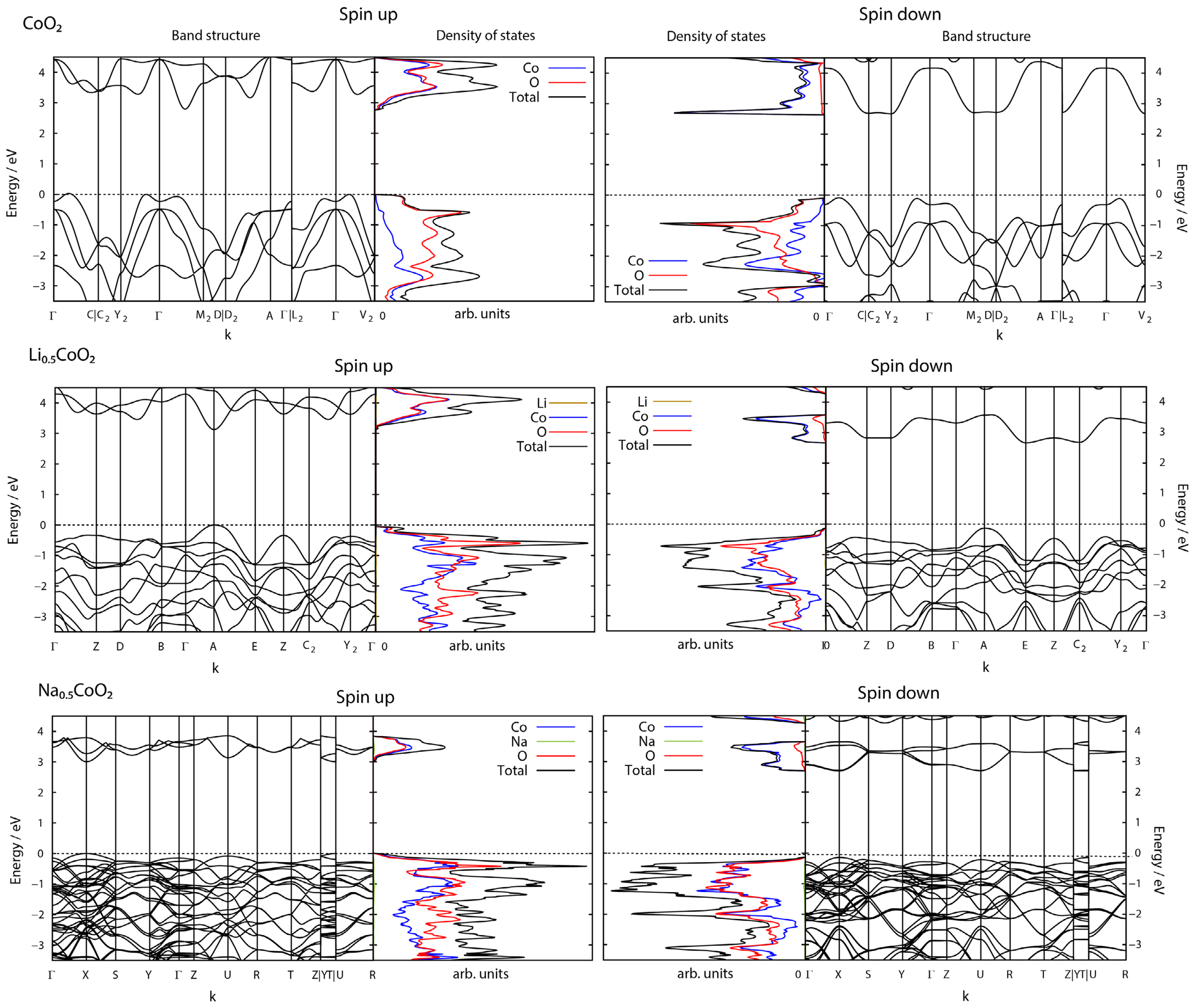

Figure 2. Electronic band structure and DOS of magnetic CoO$_2$, Li$_{0.5}$CoO$_2$, and Na$_{0.5}$CoO$_2$.

theoretical analysis of phonon properties of NaCoO$_2$ has also been carried out in space group $P6_3/mmc$ by Jha et al., but direct comparison to our results is not feasible due to lack of intensity data.[30]

For Li$_x$CoO$_2$, Inaba et al. have recorded polarized and unpolarized Raman spectra of c-axis oriented 0.8 μ_m-thick thin film at room temperature.[31] They reported two intense peaks at 486 and 596 cm^{-1} for LiCoO$_2$, which is in agreement with calculated spectra (the calculated harmonic frequencies are overestimated by about 7%). During Li deintercalation, the two peaks broadened and shifted toward lower energy. Despite the fact that a monoclinic structure has been observed for Li$_{0.5}$CoO$_2$, no additional peaks besides 475 and 575 cm^{-1} were observed. This was ascribed to random Li atom occupation.

2.4. Phonon Dispersions and DOS

The phonon dispersion relations and the phonon DOS of the studied systems are plotted in **Figure 5** and **6**. The optical modes at the Γ-point differ slightly from the infrared and Raman spectra shown above due to the nonanalytical correction term for $\mathbf{q} \to 0$ included in the phonon dispersions.

The atom-projected phonon DOS show that the high energy phonons at about 450–750 cm^{-1} are governed by oxygen and cobalt atoms, while Li and Na contribute at lower phonon energies. This is in line with the above discussion for the Γ-point phonons. In the case of CoO$_2$, there is a clear phonon bandgap between the acoustic and optical phonons at about 450 cm^{-1}. The dispersion of the acoustic phonons is clearly smaller in the Γ–A direction that corresponds to the cross-plane direction. Introducing alkali metal atoms into the interlayer space with $x = 0.5$ increases the number of phonon modes, filling up the phonon bandgap and decreasing the maximum frequency of the acoustic modes in the in-plane direction. These changes are expected to have a clear influence on the lattice thermal conductivity in the in-plane direction, as the number of phonon scattering channels increases and the phonon group velocity may

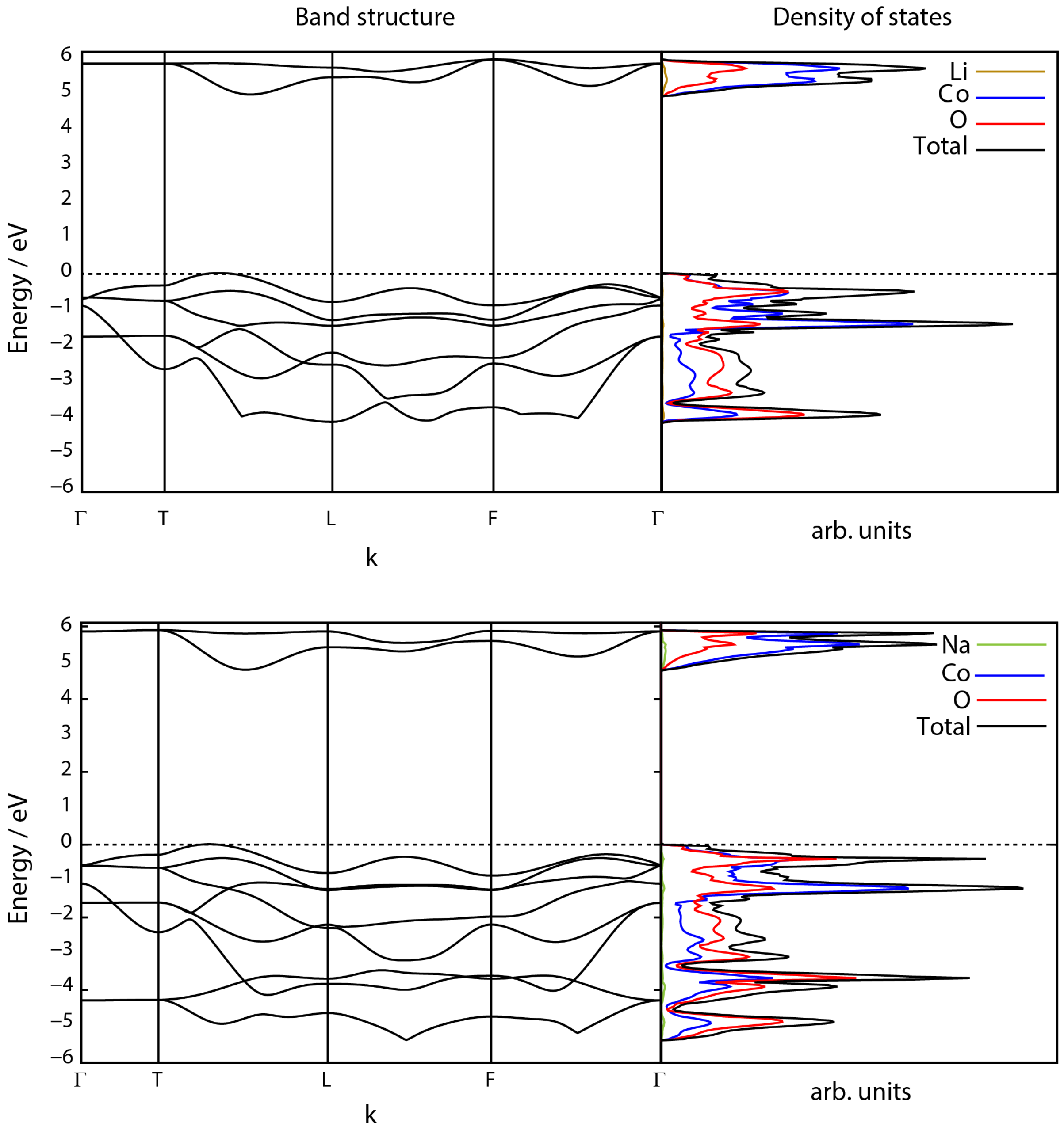

Figure 3. Electronic band structure and DOS of nonmagnetic $LiCoO_2$ (top) and $NaCoO_2$ (bottom).

decrease. For the cross-plane direction, the comparison of CoO_2 and the intercalated systems with $x = 0.5$ is not straightforward and detailed studies on the lattice thermal conductivity are needed. For the $x = 1$ systems, a phonon bandgap opens up in the case of $NaCoO_2$, while in the case of $LiCoO_2$, the Li modes prevent the opening of a phonon bandgap. To summarize, the nature of the alkali metal atom has a clear effect on the lattice dynamics of the studied M_xCoO_2 systems.

Alkali metal atom intercalation into the parent CoO_2 crystal structure has clear effects on the phonon group velocities. The largest acoustic phonon group velocity in the in-plane direction is 3.25 km s^{-1} for CoO_2 (Γ–Y_2 direction). The in-plane group velocity decreases to 2.77 and 2.79 km s^{-1} for $Li_{0.5}CoO_2$ (Γ–Y_2) and $Na_{0.5}CoO_2$ (Γ–X), respectively. For $x = 1$ systems $LiCoO_2$ and $NaCoO_2$, the in-plane group velocity in the Γ–L direction increases to 3.20 and 3.09 km s^{-1}, respectively. In the cross-plane direction, the largest acoustic phonon group velocity of CoO_2 is only 0.99 km s^{-1} (Γ–A). In the intercalated materials, the cross-plane group velocity of $Na_{0.5}CoO_2$ is lower in comparison to $Li_{0.5}CoO_2$ (1.84 vs 2.25 km s^{-1}, Γ–Z and Γ–B, respectively), but the group velocity of $NaCoO_2$ is larger in comparison to $LiCoO_2$ (2.43 vs 2.34 km s^{-1}, Γ–T for both).

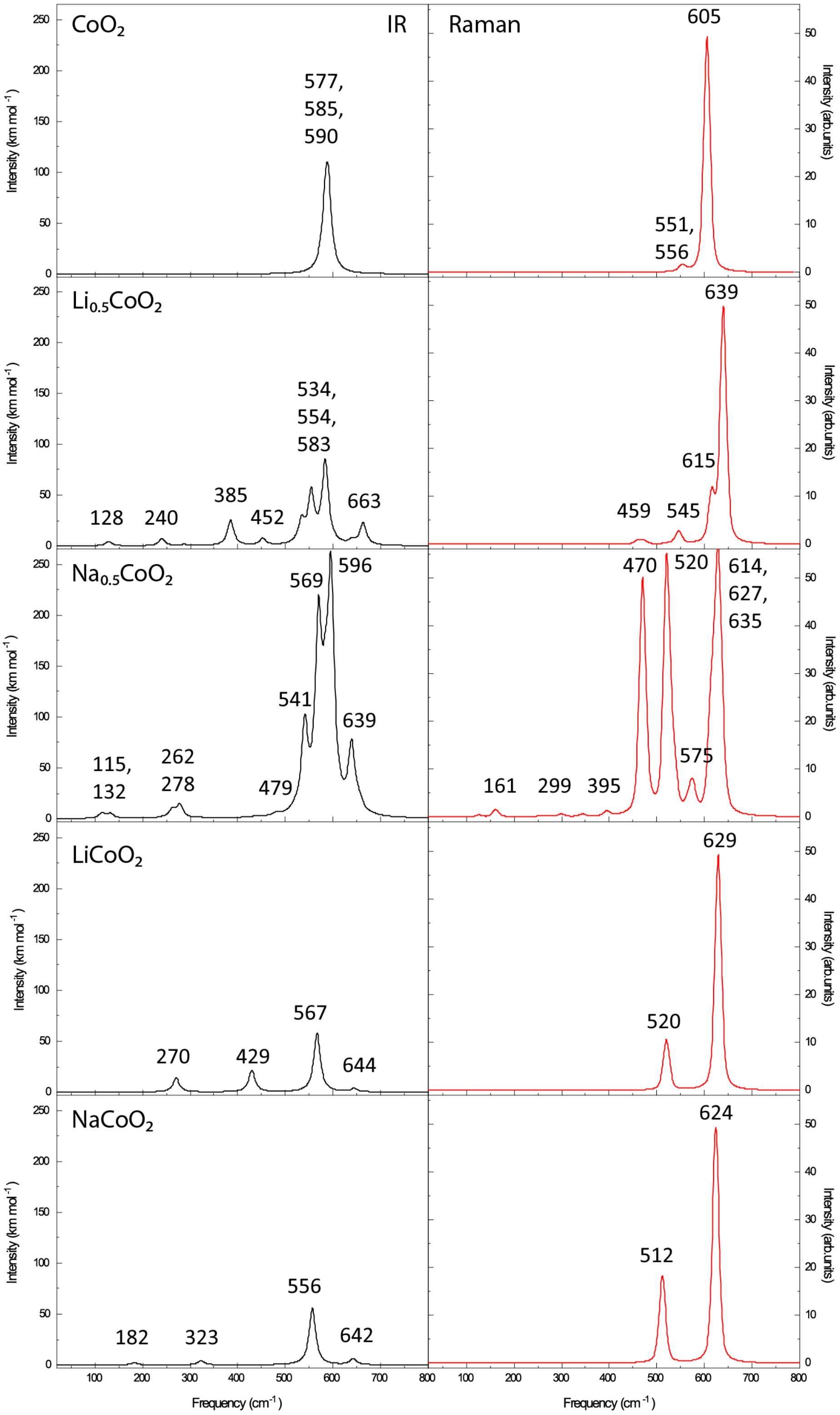

Figure 4. IR (left) and Raman (right) spectra of the studied systems. The intensity scale is different for IR and Raman spectra. LO–TO splitting has not been considered in the plotted spectra.

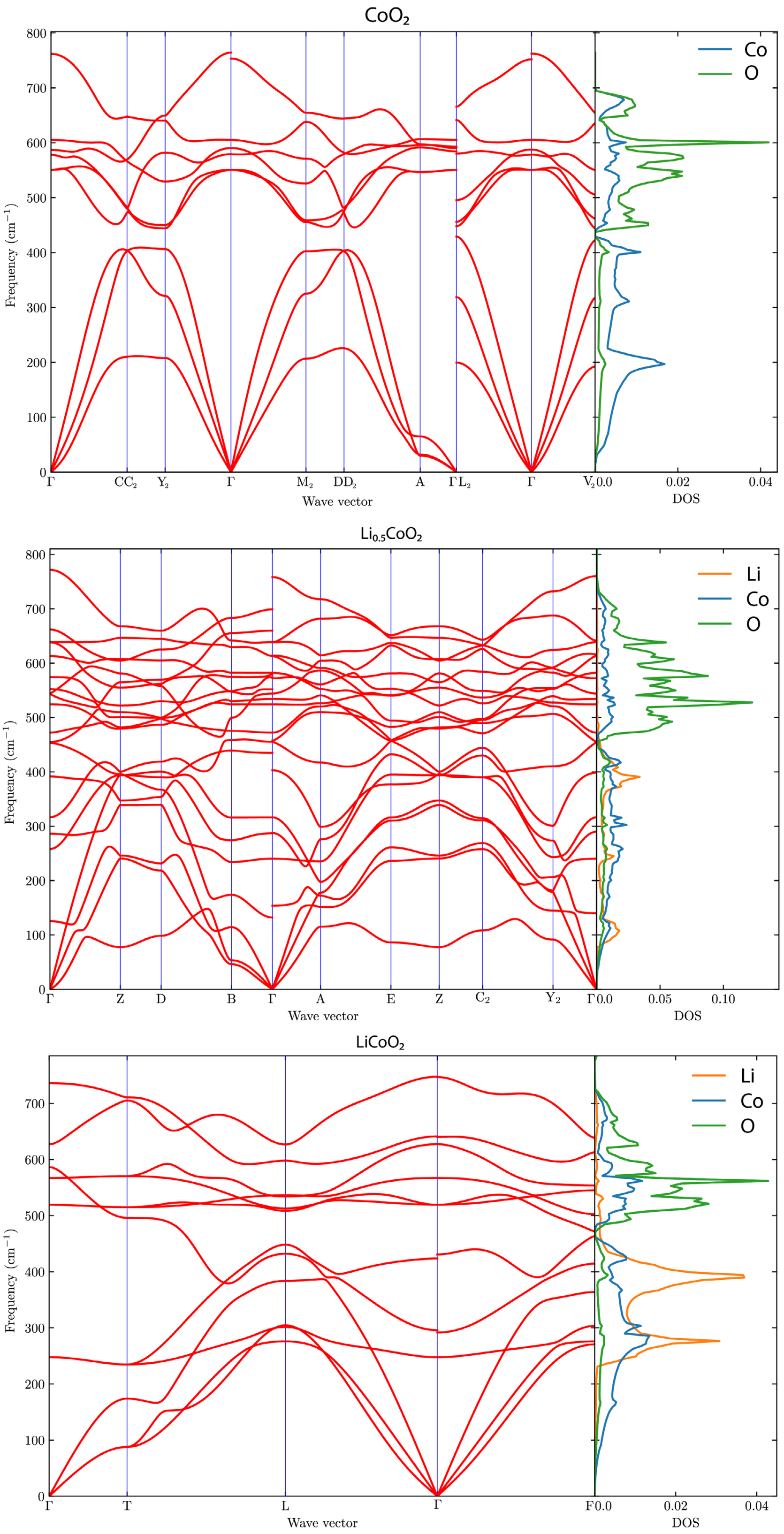

Figure 5. Phonon dispersion and density of states of CoO$_2$ and Li$_x$CoO$_2$.

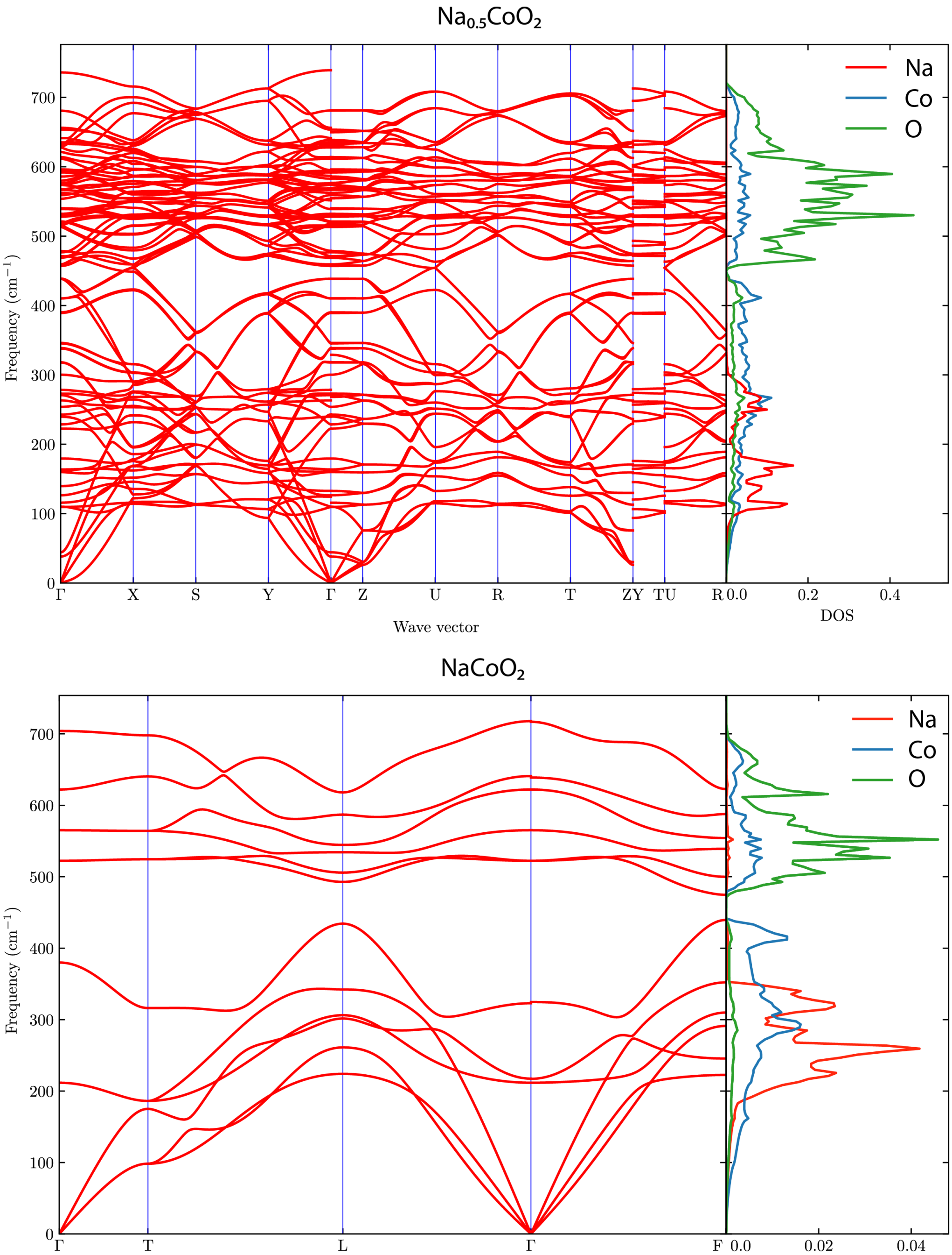

Figure 6. Phonon dispersion and density of states of Na_xCoO_2.

3. Conclusion

We have studied the electronic properties and lattice dynamics of Li_xCoO_2 and Na_xCoO_2 intercalation materials ($x = 0, 0.5, 1$) with hybrid density functional theory. The end member CoO_2 favors a monoclinic structure at 0 K and behaves in accordance with Mott insulator theory. All magnetic species were treated as ferromagnets and the Co(IV) atoms possessed a magnetic moment of 1.2 μ_B. Intercalating CoO_2 with Li and Na atoms leads to the increase of the electronic band gap and the intercalation can be observed both in IR and Raman spectra. The alkali atom intercalation also has a clear impact on the lattice dynamics of the parent CoO_2 compound, leading also in clear differences between the Li- and Na-intercalated species.

4. Computational Details

The quantum chemical calculations have been carried out using the CRYSTAL17 code and PBE0 hybrid density functional method[32–34] We applied Gaussian-type triple-ζ-valence + polarization level basis set (TZVP) for Co, O, and Li and split-valence + polarization level basis set for (SVP) for Na. The used basis sets have been derived from the molecular Karlsruhe basis sets and are identical to our previous study on fully intercalated, nonmagnetic $LiCoO_2$ and $NaCoO_2$.[24,35]

In order to take into account the weak interlayer van der Waals interactions between adjacent layers in CoO_2, we used the empirical D3 dispersion correction with zero-damping and three-body interaction term (ABC) in the geometry optimization and phonon calculations for the CoO_2 end member with $x = 0$.[36,37] The zero-damping scheme was utilized as we have previously reported the Becke–Johnson damping to overestimate the interlayer interaction in TiS_2, ZrS_2, and HfS_2.[38]

The following Monkhorst–Pack-type **k**-meshes for sampling the reciprocal space were used[39]: CoO_2: $12 \times 12 \times 8$; $Li_{0.5}CoO_2$: $8 \times 12 \times 8$; $Na_{0.5}CoO_2$: $8 \times 8 \times 4$; $LiCoO_2$ and $NaCoO_2$: $8 \times 8 \times 8$. A double-density mesh was used in the evaluation of the Fermi energy for the $x = 0$ and $x = 0.5$ systems. Obtaining the correct electronic ground state for the magnetic $x = 0$ and $x = 0.5$ systems required careful tuning of the initial guess. The full input examples with the initial guess settings are included as Supporting Information.[25] Both the atomic positions and lattice parameters were fully optimized within the constraints imposed by the space group symmetry. Default DFT integration grids and optimization convergence thresholds of CRYSTAL17 were applied in all calculations. The calculations were carried out with Coulomb and exchange integral tolerance factors (TOLINTEG) set to tight values of 8, 8, 8, 8, and 16. The phonon dispersion relations of $Li_{0.5}CoO_2$ required even tighter TOLINTEG values of 10, 10, 10, 10, and 20.

The Γ-point vibrational frequencies were obtained within the harmonic approximation by using the scheme implemented in CRYSTAL.[40,41] IR and Raman intensities for simulating vibrational spectra were obtained within the coupled perturbed Kohn–Sham method as implemented in CRYSTAL code.[42,43] The IR absorbances are reported with units of $km\ mol^{-1}$ and the spectra have been broadened by Lorenzian line shape and FWHM of $16\ cm^{-1}$. The Raman intensities are reported in arbitrary units and spectra have been broadened using pseudo-Voigt peak profile (50:50 Lorenzian:Gaussian) and FWHM of $16\ cm^{-1}$.

Phonon dispersion relations were calculated within the harmonic approximation using Phonopy code.[44] Phonopy uses a supercell approach in combination with atomic finite displacement method. Based on our previous benchmark calculations for $LiCoO_2$ and $NaCoO_2$,[24] phonon supercell dimensions of about 10 Å were considered sufficient to obtain converged phonon dispersion relations. The following phonon supercells were applied: $3 \times 3 \times 2$ for CoO_2, $3 \times 4 \times 2$ for $Li_{0.5}CoO_2$, $2 \times 2 \times 1$ for $Na_{0.5}CoO_2$, and $4 \times 4 \times 4$ for $(Li,Na)CoO_2$, respectively. The phonon supercells were created with a displacement amplitude of 0.03 Å. Nonanalytical correction (NAC) as $\mathbf{q} \rightarrow 0$ has been included in all phonon calculations using the method of Wang et al.,[45] except for $Li_{0.5}CoO_2$, where the method of Gonze et al.[46] had to be used to avoid imaginary phonon modes. $3 \times 3 \times 3$ **k**-sampling was used for $x = 0$ and $2 \times 2 \times 2$ sampling for the $x = 1$ systems. For the $x = 0.5$ case, $2 \times 3 \times 3$ and $3 \times 3 \times 3$ sampling was used for $Li_{0.5}CoO_2$ and $Na_{0.5}CoO_2$, respectively. For the lattice dynamics calculations, tight SCF convergence criterion of 10^{-10} a.u. was applied. The $Li_{0.5}CoO_2$ phonon supercell calculations required Fermi surface smearing of 0.001 a.u. (315 K) to converge. The reciprocal space coordinates used for plotting the electronic and phonon band structures were obtained from the SeeK-path service.[47–49]

Supporting Information

Supporting Information is available from the Wiley Online Library or from the author.

Acknowledgements

The authors thank the Academy of Finland for funding (grant nos. 292431 and 317273) and CSC—the Finnish IT Center for Science for computational resources.

Conflict of Interest

The authors declare no conflict of interest.

Data Availability Statement

The data that support the findings of this study are available in the supplementary material of this article.

Keywords

density functional calculations, electronic properties, lattice dynamics, layered compounds, magnetism

Received: December 27, 2021
Revised: February 2, 2022

---

[1] K. Mizushima, P. Jones, P. Wiseman, J. B. Goodenough, *Solid State Ion.* **1981**, *3*, 171.
[2] Y. Shao-Horn, S. Levasseur, F. Weill, C. Delmas, *J. Electrochem. Soc.* **2003**, *150*, A366.
[3] E. Plichta, S. Slane, M. Uchiyama, M. Salomon, D. Chua, W. B. Ebner, H. W. Lin, *J. Electrochem. Soc.* **1989**, *136*, 1865.
[4] I. Terasaki, Y. Sasago, K. Uchinokura, *Phys. Rev. B* **1997**, *56*, R12685.
[5] M. L. Foo, Y. Wang, S. Watauchi, H. W. Zandbergen, T. He, R. J. Cava, N. P. Ong, *Phys. Rev. Lett.* **2004**, *92*, 247001.
[6] T. Kawata, Y. Iguchi, T. Itoh, K. Takahata, I. Terasaki, *Phys. Rev. B* **1999**, *60*, 10584.
[7] K. Takada, H. Sakurai, E. Takayama-Muromachi, F. Izumi, R. A. Dilanian, T. Sasaki, *Nature* **2003**, *422*, 53.
[8] G. Amatucci, J. Tarascon, L. Klein, *J. Electrochem. Soc.* **1996**, *143*, 1114.
[9] K.-W. Lee, W. E. Pickett, *Phys. Rev. B* **2005**, *72*, 115110.
[10] T. Motohashi, Y. Katsumata, T. Ono, R. Kanno, M. Karppinen, H. Yamauchi, *Chem. Mater.* **2007**, *19*, 5063.

[11] C. de Vaulx, M.-H. Julien, C. Berthier, S. Hébert, V. Pralong, A. Maignan, *Phys. Rev. Lett.* **2007**, *98*, 246402.
[12] S. Kawasaki, T. Motohashi, K. Shimada, T. Ono, R. Kanno, M. Karppinen, H. Yamauchi, G.-Q. Zheng, *Phys. Rev. B* **2009**, *79*, 220514.
[13] P. Zhang, W. Luo, V. H. Crespi, M. L. Cohen, S. G. Louie, *Phys. Rev. B* **2004**, *70*, 085108.
[14] T. Tanaka, S. Nakamura, S. Iida, *Jpn. J. Appl. Phys.* **1994**, *33*, L581.
[15] R. Ray, A. Ghoshray, K. Ghoshray, S. Nakamura, *Phys. Status Solidi C* **1999**, *215*, 703.
[16] T. Motohashi, R. Ueda, E. Naujalis, T. Tojo, I. Terasaki, T. Atake, M. Karppinen, H. Yamauchi, *Phys. Rev. B* **2003**, *67*, 064406.
[17] Q. Huang, M. L. Foo, J. W. Lynn, H. W. Zandbergen, G. Lawes, Y. Wang, B. H. Toby, A. P. Ramirez, N. P. Ong, R. J. Cava, *J. Phys.: Condens. Matter* **2004**, *16*, 5803.
[18] L. Viciu, J. W. G. Bos, H. W. Zandbergen, Q. Huang, M. L. Foo, S. Ishiwata, A. P. Ramirez, M. Lee, N. P. Ong, R. J. Cava, *Phys. Rev. B* **2006**, *73*, 174104.
[19] A. J. Williams, J. P. Attfield, M. L. Foo, L. Viciu, R. J. Cava, *Phys. Rev. B* **2006**, *73*, 134401.
[20] D. J. Singh, *Phys. Rev. B* **2000**, *61*, 13397.
[21] M. Jansen, R. Hoppe, *Z. Anorg. Allg. Chem.* **1974**, *408*, 104.
[22] J. T. Hertz, Q. Huang, T. McQueen, T. Klimczuk, J. W. G. Bos, L. Viciu, R. J. Cava, *Phys. Rev. B* **2008**, *77*, 075119.
[23] T. Motohashi, T. Ono, Y. Sugimoto, Y. Masubuchi, S. Kikkawa, R. Kanno, M. Karppinen, H. Yamauchi, *Phys. Rev. B* **2009**, *80*, 16.
[24] N. Mattila, A. J. Karttunen, *Mater. Res. Express* **2020**, *8*, 075502.
[25] See Supporting Information which includes CRYSTAL input files for magnetic systems, full IR and Raman spectral data, and the optimized geometries as CIF files.
[26] H. Yang, C. Nie, Y. Shi, H. Yu, S. Ding, Y. Liu, D. Wu, N. Wang, J. Li, *Solid State Commun.* **2005**, *134*, 403.
[27] X. Zhang, P. Lemmens, V. Gnezdilov, K. Choi, B. Keimer, D. Chen, C. Lin, F. Chou, *Physica B* **2005**, *359–361*, 424 [Proceedings of the Int. Conf. on Strongly Correlated Electron Systems (SCES 2004), July 2004, Karlsruhe, Germany].
[28] N. L. Wang, D. Wu, G. Li, X. H. Chen, C. H. Wang, X. G. Luo, *Phys. Rev. Lett.* **2004**, *93*, 147403.
[29] S. Lupi, M. Ortolani, L. Baldassarre, P. Calvani, D. Prabhakaran, A. T. Boothroyd, *Phys. Rev. B* **2005**, *72*, 024550.
[30] P. K. Jha, A. Troper, I. C. da Cunha Lima, M. Talati, S. Sanyal, *Physica B* **2005**, *366*, 153.
[31] M. Inaba, Y. Iriyama, Z. Ogumi, Y. Todzuka, A. Tasaka, *J. Raman Spectrosc.* **1997**, *28*, 613.
[32] R. Dovesi, A. Erba, R. Orlando, C. M. Zicovich-Wilson, B. Civalleri, L. Maschio, M. Rérat, S. Casassa, J. Baima, S. Salustro, B. Kirtman, *WIREs Comput. Mol. Sci.* **2018**, *8*, e1360.
[33] J. P. Perdew, K. Burke, M. Ernzerhof, *Phys. Rev. Lett.* **1996**, *77*, 3865.
[34] C. Adamo, V. Barone, *J. Chem. Phys.* **1999**, *110*, 6158.
[35] F. Weigend, R. Ahlrichs, *Phys. Chem. Chem. Phys.* **2005**, *7*, 3297.
[36] S. Grimme, J. Antony, S. Ehrlich, H. Krieg, *J. Chem. Phys.* **2010**, *132*, 154104.
[37] J. Moellmann, S. Grimme, *J. Phys. Chem. C* **2014**, *118*, 7615.
[38] N. Glebko, I. Aleksandrova, G. C. Tewari, T. S. Tripathi, M. Karppinen, A. J. Karttunen, *J. Phys. Chem. C* **2018**, *122*, 26835.
[39] H. J. Monkhorst, J. D. Pack, *Phys. Rev. B* **1976**, *13*, 5188.
[40] F. Pascale, C. M. Zicovich-Wilson, F. L. Gejo, B. Civalleri, R. Orlando, R. Dovesi, *J. Comput. Chem.* **2004**, *25*, 888.
[41] C. M. Zicovich-Wilson, F. Pascale, C. Roetti, V. R. Saunders, R. Orlando, R. Dovesi, *J. Comput. Chem.* **2004**, *25*, 1873.
[42] L. Maschio, B. Kirtman, M. Rérat, R. Orlando, R. Dovesi, *J. Chem. Phys.* **2013**, *139*, 164102.
[43] L. Maschio, B. Kirtman, M. Rérat, R. Orlando, R. Dovesi, *J. Chem. Phys.* **2013**, *139*, 164101.
[44] A. Togo, I. Tanaka, *Scr. Mater.* **2015**, *108*, 1.
[45] Y. Wang, J. J. Wang, W. Y. Wang, Z. G. Mei, S. L. Shang, L. Q. Chen, Z. K. Liu, *J. Phys.: Condens. Matter* **2010**, *22*, 202201.
[46] X. Gonze, C. Lee, *Phys. Rev. B* **1997**, *55*, 10355.
[47] A. Togo, I. Tanaka, *Spglib: A Software Library for Crystal Symmetry Search*, **2018**, https://arxiv.org/abs/1808.01590 (accessed: January 2022).
[48] Y. Hinuma, G. Pizzi, Y. Kumagai, F. Oba, I. Tanaka, *Comput. Mater. Sci.* **2017**, *128*, 140.
[49] https://www.materialscloud.org/work/tools/seekpath, https://www.materialscloud.org/work/tools/seekpath (accessed: January 2022).
[50] J. Akimoto, Y. Gotoh, Y. Oosawa, *J. Solid State Chem.* **1998**, *141*, 298.
[51] Y. Takahashi, Y. Gotoh, J. Akimoto, *J. Solid State Chem.* **2003**, *172*, 22.